

vanishing tassel2 Encodes a Grass-Specific Tryptophan Aminotransferase Required for Vegetative and Reproductive Development in Maize

Kimberly A. Phillips,^a Andrea L. Skirpan,^a Xing Liu,^b Ashley Christensen,^c Thomas L. Slewinski,^a Christopher Hudson,^a Solmaz Barazesh,^a Jerry D. Cohen,^b Simon Malcomber,^c and Paula McSteen^{a,1,2}

^aDepartment of Biology, Pennsylvania State University, 208 Mueller Lab, University Park, Pennsylvania 16802

^bDepartment of Horticultural Science and the Microbial and Plant Genomics Institute, University of Minnesota, Saint Paul, Minnesota 55108

^cDepartment of Biological Sciences, California State University, Long Beach, California 90840

Auxin plays a fundamental role in organogenesis in plants. Multiple pathways for auxin biosynthesis have been proposed, but none of the predicted pathways are completely understood. Here, we report the positional cloning and characterization of the *vanishing tassel2* (*vt2*) gene of maize (*Zea mays*). Phylogenetic analyses indicate that *vt2* is a co-ortholog of TRYPTOPHAN AMINOTRANSFERASE OF ARABIDOPSIS1 (*TAA1*), which converts Trp to indole-3-pyruvic acid in one of four hypothesized Trp-dependent auxin biosynthesis pathways. Unlike single mutations in *TAA1*, which cause subtle morphological phenotypes in *Arabidopsis thaliana*, *vt2* mutants have dramatic effects on vegetative and reproductive development. *vt2* mutants share many similarities with *sparse inflorescence1* (*spi1*) mutants in maize. *spi1* is proposed to encode an enzyme in the tryptamine pathway for Trp-dependent auxin biosynthesis, although this biochemical activity has recently been questioned. Surprisingly, *spi1 vt2* double mutants had only a slightly more severe phenotype than *vt2* single mutants. Furthermore, both *spi1* and *vt2* single mutants exhibited a reduction in free auxin levels, but the *spi1 vt2* double mutants did not have a further reduction compared with *vt2* single mutants. Therefore, both *spi1* and *vt2* function in auxin biosynthesis in maize, possibly in the same pathway rather than independently as previously proposed.

INTRODUCTION

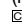
Auxin has been shown to play a critical role in all stages of plant development. Through its functions in cell division and cell expansion, auxin is required for the initiation of lateral roots, vascular strands, leaves, flowers, and floral organs (Benjamins and Scheres, 2008). Evidence from genetics, molecular biology, and modeling has shown that auxin transport is crucial for providing the source of auxin required for organogenesis (Petrásek and Friml, 2009). More recently, the importance of auxin biosynthesis in providing a localized source of auxin for organogenesis has been appreciated (Chandler, 2009).

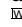
In plants, there are hypothesized to be four Trp-dependent and one Trp-independent pathway for the biosynthesis of auxin in its most common form, indole-3-acetic acid (IAA) (Figure 1) (Bartel, 1997; Woodward and Bartel, 2005; Pollmann et al., 2006; Kriechbaumer et al., 2008; Sugawara et al., 2009; McSteen,

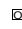
2010). Each pathway is named after an intermediate that it is proposed to use, but few genes encoding enzymes in each pathway have been identified. Therefore, none of the proposed pathways have been fully elucidated with respect to all the intermediates formed nor is it clear how the pathways might intersect with each other. (1) The IAM pathway. The conversion of Trp to IAA through an indole-3-acetamide (IAM) intermediate has been demonstrated in *Arabidopsis thaliana* (Pollmann et al., 2009). Genes encoding enzymes that catalyze the conversion of Trp to IAM are unknown, but *AMIDASE1* (*AMI1*), which converts IAM to IAA, has been identified in *Arabidopsis* (Pollmann et al., 2003). A maize (*Zea mays*) sequence with similarity to *AMI1* has recently been reported, but function has not yet been demonstrated (Lehmann et al., 2010). (2) The IAOx pathway. Genes encoding the cytochrome P450 enzymes, *CYP79B2/CYP79B3*, which convert Trp to indole-3-acetaldoxime (IAOx) have been identified in *Arabidopsis* but are not present outside of the Brassicaceae (Zhao et al., 2002; Sugawara et al., 2009). IAOx is converted to indole-3-acetonitrile by unknown means, and indole-3-acetonitrile is converted to IAA by nitrilases. Genes encoding nitrilases have been identified from both maize and *Arabidopsis* (Bartling et al., 1992; Park et al., 2003; Kriechbaumer et al., 2007). However, the existence of this pathway in maize has been questioned due to the absence of genes co-orthologous to *CYP79B2/3* genes and the lack of detectable IAOx levels (Sugawara et al., 2009). (3) The tryptamine (TAM) pathway. The enzymes converting Trp to TAM are not known, but the conversion of TAM to *N*-hydroxyl tryptamine is reported to be catalyzed

¹ Address correspondence to mcsteenp@missouri.edu.

² Current address: Division of Biological Sciences, 371 Bond Life Sciences Center, University of Missouri, Columbia, MO 65211. The author responsible for distribution of materials integral to the findings presented in this article in accordance with the policy described in the Instructions for Authors (www.plantcell.org) is: Paula McSteen (mcsteenp@missouri.edu).

 Some figures in this article are displayed in color online but in black and white in the print edition.

 Online version contains Web-only data.

 Open Access articles can be viewed online without a subscription. www.plantcell.org/cgi/doi/10.1105/tpc.110.075267

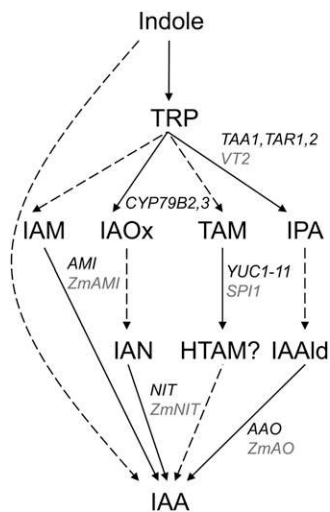


Figure 1. Proposed Auxin Biosynthesis Pathways in *Arabidopsis* and Maize.

One Trp-independent and four Trp-dependent pathways have been proposed. Dotted lines indicate steps that are inferred. Solid lines indicate steps for which genes encoding enzymes catalyzing the reaction have been identified from either *Arabidopsis* (black) or maize (gray). IAN, indole-3-acetonitrile; HTAM, *N*-hydroxyl tryptamine. Adapted from Bartel (1997), Woodward and Bartel (2005), Kriechbaumer et al. (2006), and Sugawara et al. (2009).

in vitro by the *YUCCA* (*YUC*) genes of *Arabidopsis*, which play important roles in various aspects of development (Zhao et al., 2001; Cheng et al., 2006, 2007a). However, the biochemical function of *YUC* and, in particular, the role of *N*-hydroxyl tryptamine have been called into question recently, indicating that further in vivo research is needed (Tivendale et al., 2010; Nonhebel et al., 2011). In maize, the *sparse inflorescence1* (*spi1*) gene, a monocot-specific member of the *YUC* gene family, shows that this pathway is also important for maize inflorescence development (Gallavotti et al., 2008b). Another member of the gene family (*Zm-YUC1*, which is more similar to *At-YUC10* and *At-YUC11*) is specifically expressed in endosperm, illustrating the tissue-specific regulation of the gene family (LeClere et al., 2010). (4) The IPA pathway. Trp is converted to indole-3-pyruvic acid (IPA) by TRYPTOPHAN AMINOTRANSFERASE OF ARABIDOPSIS1 (*TAA1*) and related proteins, *TAR1* and *TAR2* (Stepanova et al., 2008; Tao et al., 2008; Yamada et al., 2009). It is not known how IPA is converted to indole-3-acetaldehyde (IAAld), but the conversion of IAAld to IAA is catalyzed by aldehyde oxidases, which have been identified in both maize and *Arabidopsis* (Sekimoto et al., 1997, 1998). Here, we identify *vanishing tassel2* (*vt2*), a maize co-ortholog of *TAA1/TAR1/TAR2*.

taa1 mutants were identified in three different genetic screens in *Arabidopsis*, as indicated by the different phenotypes and nomenclature of respective mutants: insensitivity to ethylene-induced root shortening, *weak ethylene insensitive8* (Stepanova et al., 2008); insensitivity to shade-induced hypocotyl elongation, *shade avoidance3* (Tao et al., 2008); and insensitivity to naphthylphthalamic acid-induced root shortening, *transport inhibitor*

response2 (Yamada et al., 2009). Unlike the mild phenotype of *taa1* single mutants, double mutants with the paralogous gene *tar2* show more severe defects, producing dwarf, bushy plants with agravitropic roots, reduced vasculature, and sterile flowers (Stepanova et al., 2008). *taa1 tar1 tar2* triple mutants lack roots and are seedling lethal, similar to the phenotype of plants containing quadruple knockouts of the *YUC* gene family (Cheng et al., 2007a; Stepanova et al., 2008). Therefore, both the *TAA1* and *YUC* gene families exhibit genetic redundancy and function in auxin biosynthesis, which raises the question of why neither pathway can compensate for the other.

Developmental defects are also seen in mutants with altered auxin transport. For example, mutations in the auxin efflux carrier *PINFORMED1* (*PIN1*) and the *PINOID* (*PID*) kinase, which regulates *PIN1* subcellular localization, produce an inflorescence with no flowers known as a pin inflorescence (Bennett et al., 1995; Gälweiler et al., 1998; Christensen et al., 2000; Friml et al., 2004; Kleine-Vehn et al., 2009; Zhang et al., 2010). Mutations in the *PID* co-ortholog in maize, *barren inflorescence2* (*bif2*), result in an equivalent phenotype called a barren inflorescence (*bif*) phenotype: no branches and few spikelets (small branches that bear the florets) are produced in the male inflorescence (the tassel), and few kernels are produced in the female inflorescence (the ear) (McSteen and Hake, 2001). Fewer flowers are also seen in *yuc1 yuc2* double mutants in *Arabidopsis* and *spi1* single mutants in maize (Cheng et al., 2006; Gallavotti et al., 2008b), indicating that both auxin transport and auxin biosynthesis are required for the initiation of flowers. The importance of these two processes in development is further illustrated by the synergistic interactions observed between auxin biosynthesis and transport mutants. For example, *yuc1 yuc4 pin1* triple mutants do not produce leaves, and *spi1 bif2* double mutants have dramatically reduced leaf number, indicating that both auxin biosynthesis and transport are required for leaf initiation in addition to flower initiation (Cheng et al., 2007a; Gallavotti et al., 2008b).

Here, we report on the identification of the *vt2* mutant of maize, which exhibits a severe barren inflorescence phenotype with no branches or spikelets, as well as a semidwarf vegetative phenotype due to the production of fewer leaves. Positional cloning and phylogenetic analysis indicate that *vt2* encodes a co-ortholog of the *TAA1/TAR1/TAR2* genes of *Arabidopsis*, which function in the IPA pathway for auxin biosynthesis (Stepanova et al., 2008; Tao et al., 2008; Yamada et al., 2009). The dramatic phenotype of *vt2* loss-of-function mutants indicates that the IPA pathway plays a critical role in maize vegetative and reproductive development. Furthermore, due to the reduced redundancy of the *vt2* and *spi1* genes in maize, we were able to test the relative contributions of the IPA and TAM pathways to auxin biosynthesis.

RESULTS

vt2 Functions in Vegetative Development

At maturity, *vt2* mutants were visibly shorter than wild-type siblings (Figure 2A). As expected, quantification revealed a statistically significant reduction in plant height in *vt2* mutants compared with the wild-type (Figure 2B). To determine if this

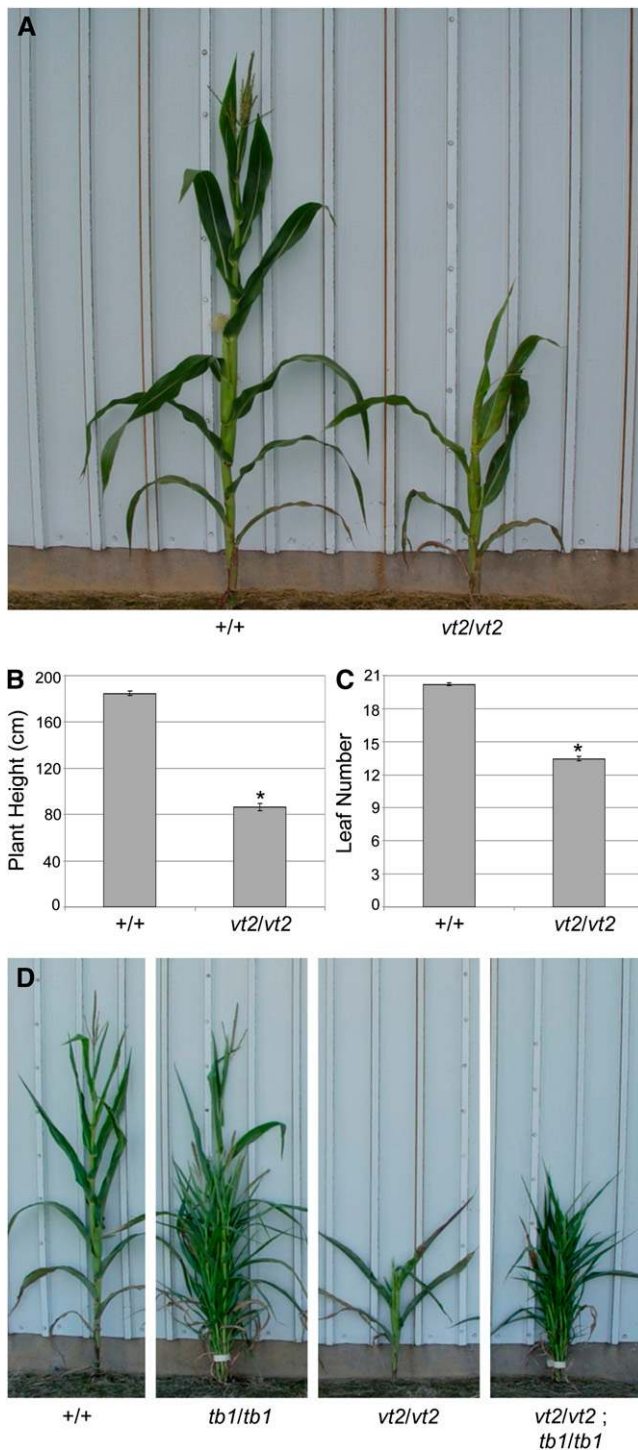


Figure 2. Mature Vegetative Phenotype Analysis of *vt2* Mutants.

(A) *vt2* mutants are much shorter than their wild-type siblings.
 (B) Quantification of plant height.
 (C) Quantification of leaf number.
 (D) Mature vegetative phenotypes of individuals from a segregating *vt2* *tb1* double mutant family show that *vt2/vt2* *tb1/tb1* double mutants produce many tillers like *tb1/tb1* single mutants. Asterisk indicates

decrease in plant height was caused by a reduction in the number of leaves produced, leaf number was counted. Wild-type maize plants produced an average of $20.2 (\pm 0.1 \text{ SE})$ leaves at maturity, whereas *vt2* mutants produced $\sim 13.5 (\pm 0.18 \text{ SE})$ leaves (Figure 2C). Therefore, the reduction in plant height in *vt2* is due in part to a reduction in leaf number, although reduced tassel length also contributes to the reduced plant height (see below).

The decrease in leaf number in *vt2* mutants could be due to the production of fewer juvenile leaves or fewer adult leaves. To determine which leaves were missing in *vt2* mutants, the juvenile-to-adult transition was analyzed through visual inspection of leaf waxes. Due to the production of epicuticular waxes, the surface of juvenile maize leaves appears dull while adult leaves appear glossy, and transitional leaves (with a glossy appearance at the tip and a matte appearance at the base and margins) are produced at the juvenile-to-adult transition (Kerstetter and Poethig, 1998). In wild-type siblings, the juvenile-to-adult transition began at leaf six when transitional leaves were produced, and the transition continued through leaf eight after which adult glossy leaves were produced (see Supplemental Table 1 online). *vt2* mutants showed no substantial difference in the transition point from juvenile to transitional leaves or from transitional leaves to adult leaves (see Supplemental Table 1 online). As there is no difference in the timing of the juvenile-to-adult transition in *vt2* mutants, this indicates that the later-formed adult leaves are those that are missing in *vt2* mutants.

vt2 Functions in Inflorescence Development

In maize, the tassel inflorescence normally produces a main spike with several long lateral branches extending near the base (Figure 3A) (McSteen et al., 2000). Short branches known as spikelet pairs house the florets and cover both the main spike and long branches (Figure 3A). *vt2* mutant tassels were smaller at maturity and exhibited a severely barren phenotype compared with wild-type siblings, including a complete lack of lateral branches and functional spikelets (Figure 3A). Quantitative analysis of tassel length (Figure 3B), branch number (Figure 3C), and spikelet number (Figure 3D) confirmed a significant reduction in *vt2* mutants compared with the wild type.

Reduction in tassel length in other barren inflorescence mutants has been shown to be caused by reduced cell size (Barazesh et al., 2009). To test whether the reduction in tassel length in *vt2* was caused by a reduction in cell size, the length of cells in the epidermis of the mature tassel was measured. *vt2* mutants exhibited a 63% reduction in epidermal cell length compared with normal siblings (see Supplemental Table 2 online). Therefore, the reduced tassel length in *vt2* mutants is likely due to reduced cell elongation.

In addition to male inflorescence defects, *vt2* mutants also showed severe defects in the female inflorescence. *vt2* mutant ears showed obvious defects in length and kernel number with a

significant reduction from normal siblings at $P < 0.05$; error bars represent the SE; $n = 37$ *vt2* and 113 normal.

[See online article for color version of this figure.]

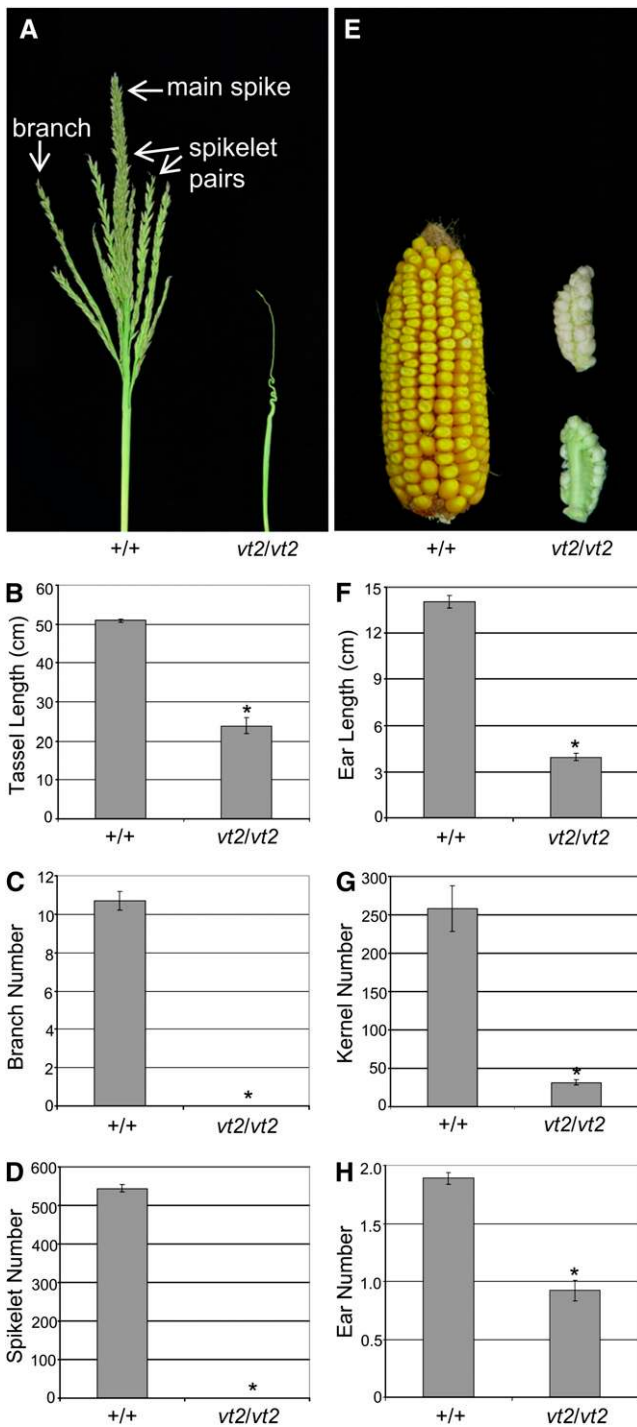


Figure 3. Mature Inflorescence Phenotype Analysis of *vt2* Mutants. (A) Wild-type tassels normally produce multiple lateral branches. The branches and the main spike are covered in pairs of spikelets. *vt2* mutant tassels produce no lateral branches or functional spikelets. (B) Quantification of tassel length. (C) Quantification of tassel branch number. (D) Quantification of spikelet number in the tassel. (E) Wild-type ears normally produce hundreds of kernels in regular rows

barren patch devoid of kernels often extending along the adaxial side of the ear (Figure 3E). Quantification of traits at maturity revealed a statistically significant reduction in both ear length (Figure 3F) and kernel number (Figure 3G) in *vt2* mutants compared with the wild type. In addition, segregating families were scored to determine if the number of visible ear shoots produced by *vt2* mutants was altered compared with wild-type siblings, and a statistically significant reduction in *vt2* ear shoot number was detected (Figure 3H). These data show that *vt2* ear inflorescences exhibit similar defects to those observed in tassel inflorescences and together indicate that *vt2* plays an important role in inflorescence development. As all of the reproductive structures missing arise from axillary meristems (ear shoots, tassel branches, spikelets, and kernels), it appears that *vt2* mutants are defective in axillary meristem formation similar to other maize mutants with defects in auxin transport or biosynthesis (McSteen and Hake, 2001; Barazesh and McSteen, 2008; Gallavotti et al., 2008b).

vt2 Functions in Axillary Meristem Formation during Inflorescence Development

To determine whether the absence of branches and spikelets in *vt2* inflorescences was caused by altered axillary meristem formation, we observed tassel inflorescences at early stages of development using scanning electron microscopy. Early in development, wild-type tassels produce branch meristems (BMs) at the base of the inflorescence and spikelet pair meristems (SPMs) in regular rows on the flanks of both the branches and main spike (Figure 4A, arrows) (Cheng et al., 1983). By contrast, field-grown *vt2* mutant tassels showed a complete lack of formation of both BMs and SPMs early in development (Figure 4B). Later in development, a few SPMs formed sporadically near the tip of the inflorescence (Figure 4C). Scanning electron microscopy was also performed on developing ear inflorescences, and similar defects in axillary meristem formation were observed (see Supplemental Figure 1 online).

Although field-grown *vt2* mutant tassels never produced functional spikelets, we observed that temperature conditions during development greatly impacted the severity of the phenotype. In *vt2* mutant tassels grown under typical warm maize greenhouse growing conditions, we observed a very weak phenotype with the production of several BMs and many irregularly placed SPMs (Figure 4D). To explore the role of temperature in *vt2* inflorescence development further, we grew plants under normal warm and cooler greenhouse growing conditions until later in development.

from the base to the tip, whereas *vt2* mutant ears are smaller in size, produce very few kernels, and typically have barren patches on one or both sides of the ear (both sides of the same *vt2* ear are shown on the right).

(F) Quantification of ear length. (G) Quantification of kernel number. (H) Quantification of visible ear shoot number. Asterisk indicates significant reduction compared with normal siblings at $P < 0.05$; error bars represent the SE; $n = 10$ *vt2* and 10 normal. [See online article for color version of this figure.]

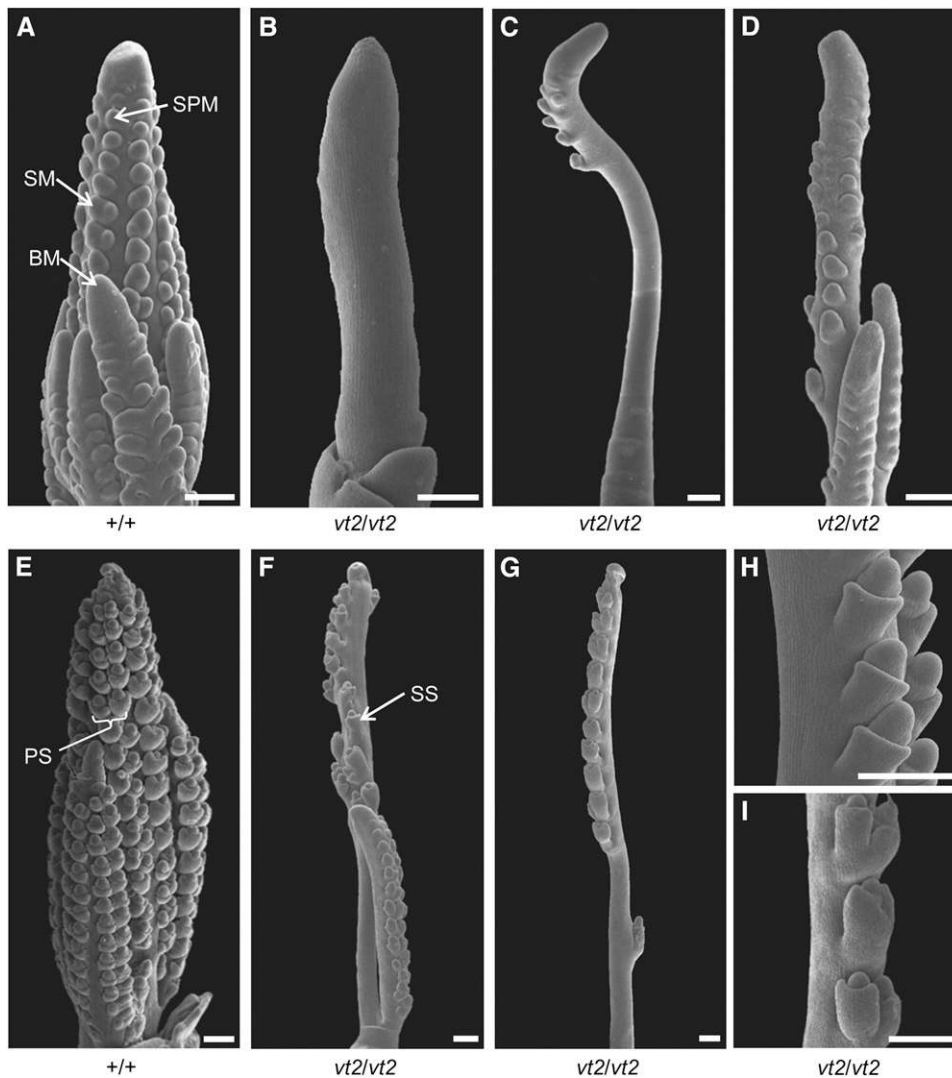


Figure 4. Scanning Electron Micrographs of Developing Inflorescences.

(A) Wild-type field-grown tassel at 3-mm stage exhibiting BMs at the base and SPMs covering the branches and main spike.

(B) *vt2* field-grown tassel at 3-mm stage exhibiting complete lack of BM and SPM initiation.

(C) *vt2* field-grown tassel at 4- to 5-mm stage producing a few SPMs near the tip.

(D) *vt2* greenhouse-grown tassel at 4- to 5-mm stage displaying a weak mutant phenotype, with several BMs at the base and many SPM on the branches and main spike.

(E) Wild-type greenhouse-grown tassel later in development at 6- to 7-mm stage exhibiting production of paired SMs in regular rows on all branches and the main spike.

(F) *vt2* greenhouse-grown tassel later in development at 6- to 7-mm stage showing production of paired SMs on the branches and paired or single SMs on the main spike.

(G) *vt2* mutant tassel at 6- to 7-mm stage grown at cooler greenhouse temperatures compared with typical greenhouse conditions for maize. Mutants grown in these conditions display intermediate phenotypes between field-grown and typical greenhouse-grown tassels, with no BMs and few SPMs, which give rise to paired or single SM.

(H) Close-up of 4- to 5-mm *vt2* tassel grown at cooler greenhouse temperatures, displaying two files of single SMs produced along the main spike.

(I) Close-up of 6- to 7-mm *vt2* tassel (from **[G]**) grown at cooler greenhouse temperatures, displaying both paired and single SMs along the main spike.

PS, paired spikelet; SS, single spikelet. Bars = 250 μ m.

In wild-type greenhouse-grown plants, SPMs on the branches and main spike gave rise to two spikelet meristems (SMs) (Figures 4A and 4E). *vt2* mutants grown in warm greenhouse conditions produced both single and paired SMs (Figure 4F), which is characteristic of barren inflorescence mutants in maize (McSteen and Hake, 2001; Barazesh and McSteen, 2008). However, *vt2* mutants grown in cooler greenhouse conditions had a more severe phenotype in which BMs were typically not produced, and the SPMs that were produced often gave rise to single SMs (Figures 4G to 4I). Hence, in cooler greenhouse conditions, the *vt2* mutant phenotype was more severe than that observed under warmer greenhouse conditions, although the most severe phenotypes were seen in field-grown plants that were exposed to very cold minimum nighttime temperatures (see Methods).

Therefore, *vt2* mutants produce few branches and spikelets due to defects in BM, SPM, and SM formation. Furthermore, the phenotype is temperature dependent. In addition to *vt2-ref*, this temperature dependence was also observed in the *vt2-RM123* and *vt2-DB1845* alleles; hence, this phenomenon is not due to *vt2-ref* being a temperature-sensitive allele.

vt2 Does Not Function in Axillary Meristem Formation during Vegetative Development

As *vt2* played an important role in axillary meristems during inflorescence development, we also tested the role of *vt2* in axillary meristems during vegetative development by constructing double mutants with *teosinte branched1* (*tb1*). The *tb1* gene functions to suppress the outgrowth of branches (tillers) from vegetative axillary meristems located in the axil of each leaf node (Doebley et al., 1997; Hubbard et al., 2002). Loss of function of *tb1* allows the outgrowth of vegetative axillary meristems, resulting in mutants that produce many tillers (Figure 2D). *vt2 tb1* double mutants had an additive phenotype, producing short plants with many tillers topped by *vt2* tassels (Figure 2D). Quantification of tiller number on the main stem indicated no statistical difference between the number of tillers in *tb1* (9.65 ± 0.69) compared with *vt2 tb1* (9.78 ± 1.29 , P value = 0.922). This additive genetic interaction indicates that *vt2* does not play a role in axillary meristem formation during vegetative development. Furthermore, the production of a similar number of tillers in *tb1* and *vt2 tb1* provides further support that later arising leaves are missing in *vt2* mutants, as *tb1* mutants do not produce tillers from the uppermost nodes.

Positional Cloning of vt2

vt2 was proposed to be allelic to the semidominant *Bif1* mutant (Smith and Hake, 1993); however, allelism tests revealed that the two genes were not allelic, but closely linked on chromosome 8L. To define the map position of *vt2* further, two F2 mapping populations, *vt2-ref*-B73 \times Mo17 and *vt2-TR799*-A619 \times B73, were constructed. Using simple sequence repeat and insertion-deletion polymorphism markers, *vt2* was fine-mapped to within two BAC contigs in bin 8.02. Marker *idp98* was identified as the closest public flanking marker available on the north side of *vt2* (1.36 centimorgans [cM], contig 326), and *umc1974* was identified as the closest public marker on the south side of *vt2* (0.12

cM, contig 327) (Figure 5A). Between these two flanking markers, a third public marker, *umc1872*, was found to be polymorphic but did not detect any recombinants, indicating that it was tightly linked to the mutant (0 cM, contig 327). Using single nucleotide polymorphism (SNP) markers identified in neighboring genes in the region, the number of recombinants on the north (*idp98*) side was narrowed down (WD1 SNP, 0.22 cM), placing *vt2* on contig 327 within a region containing three overlapping BAC clones (Figure 5A). A candidate gene search in the region revealed a Trp aminotransferase-like gene (Stepanova et al., 2008; Tao et al., 2008; Yamada et al., 2009) located on the overlapping portion of two of the three BAC clones (Figure 5A).

To test if the Trp aminotransferase-like candidate gene was *vt2*, overlapping gene-specific PCR primers (see Supplemental Table 3 online) were designed to amplify and sequence the gene from all *vt2* alleles. Point mutations that were not present in the progenitor backgrounds were identified in the coding regions of each of four ethyl methanesulfonate (EMS)-induced alleles, three of which caused a single amino acid substitution and one of which caused a premature stop codon in the predicted protein (Figures 5B and 5C). PCR amplification of the *vt2-DB1845* allele using primers near the 3' end of the gene revealed an insertion of ~ 300 bp in the 5th exon (Figure 5B). The *Mutator* (*Mu*) transposon-induced alleles, *vt2-ref* and *vt2-RM123*, were screened with a conserved *Mu* terminal inverted repeat primer (*Mu3456*) and gene-specific primers to identify potential *Mu* insertions. Sequencing of the PCR products revealed a *Mu1* insertion in the first exon of *vt2-RM123* and in the first intron of *vt2-ref* (Figure 5B). The *vt2-ref* allele was also determined to have a 12-amino acid deletion in the second exon (Figures 5B and 5C). These data indicate significant sequence changes in seven independent alleles and confirm that the *vt2* gene encodes a Trp aminotransferase.

vt2 Is Co-Orthologous to Trp Aminotransferases from Arabidopsis

Sequence analysis of *vt2* revealed highest similarity to the Trp aminotransferase gene of *Arabidopsis*, *TAA1*, and two Trp aminotransferase-related genes, *TAR1* and *TAR2* (Figure 5C) (Stepanova et al., 2008; Tao et al., 2008; Yamada et al., 2009). These genes have been categorized in the superfamily of pyridoxal-5'-phosphate-dependent enzymes, which differ from typical alliinases like *TAR3* and *TAR4* by their lack of an epidermal growth factor domain (Stepanova et al., 2008; Tao et al., 2008). The similarity between VT2 and the founding member of the alliinase family, garlic (*Allium sativum*) alliinase, extends throughout most of the coding region of VT2 containing the alliinase C-terminal domain (35% amino acid identity). Sequence alignment in this region indicated that VT2 shares 51% amino acid identity with *TAA1*, 51% identity with *TAR1*, and 56% identity with *TAR2*. The predicted amino acid sequence of VT2 is 90 amino acids longer than the longest *Arabidopsis* gene *TAR2* due to an extended N terminus. Sequence alignment also indicated that the *vt2* EMS-induced alleles and the *vt2-ref* deletion caused mutations in regions conserved with garlic alliinase and the *TAA1/TAR* genes from *Arabidopsis*. Notably, the *vt2-GN21* allele had an Arg to Trp amino acid substitution at one of the known enzyme active sites (Kuettner et al., 2002; Tao

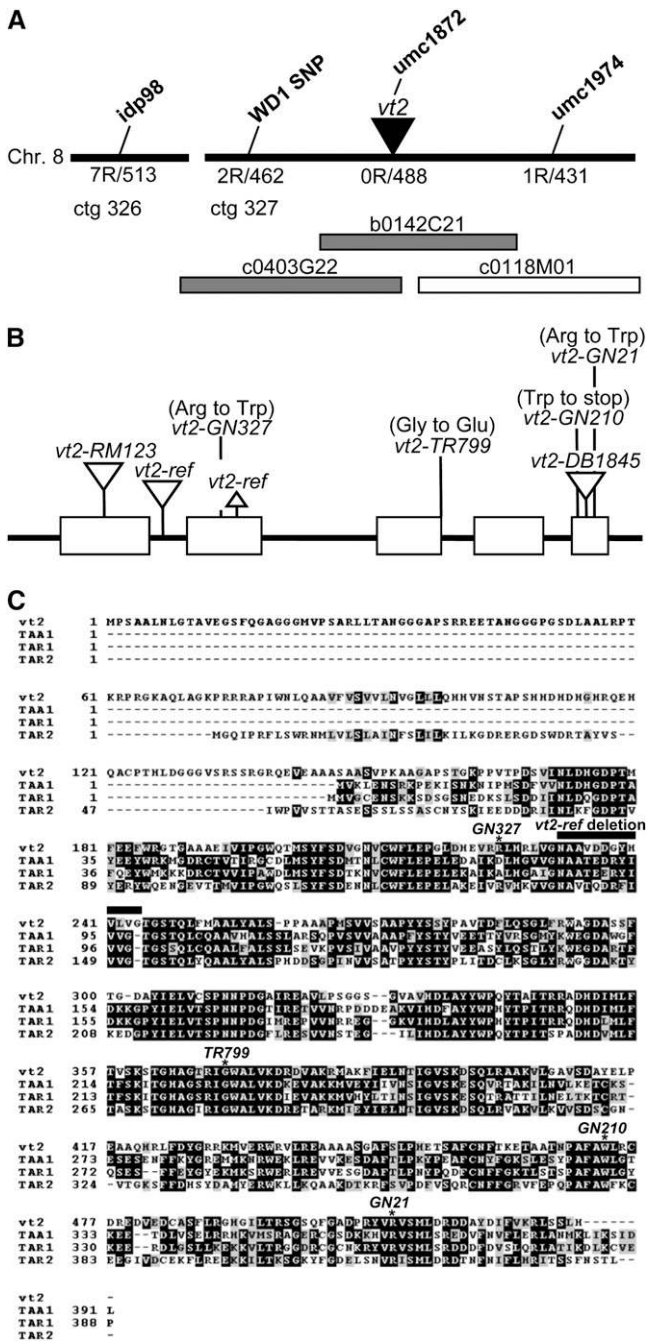


Figure 5. Cloning and Sequence Analysis of *vt2*.

(A) Diagram representing the *vt2* region in maize after mapping with public and SNP markers (not to scale). The number of recombinant chromosomes (R) out of the total number of chromosomes is displayed below each marker. Maize BAC clones within this region are represented by rectangles, with the shaded rectangles indicating the overlapping clones on which *vt2* was identified.

(B) Schematic of the *vt2* gene structure including the position and mutations of seven alleles. Exons are represented by boxes; insertions and deletions are represented by downward and upward triangles, respectively.

et al., 2008). As all alleles have a similar phenotype to that of *vt2-GN21*, all alleles are assumed to be null.

Bayesian phylogenetic analysis of 82 land plant and fungal alliinases recovered two major clades of Trp aminotransferases that are estimated products of a duplication event prior to the origin of extant land plants ~450 million years ago (Sanderson, 2003) (Figure 6). The first clade comprised liverwort (*Marchantia*), moss (*Physcomitrella*), gymnosperm (*Pinus* and *Picea*), and flowering plant sequences, including *Arabidopsis* TAA1/TAR1/TAR2 and maize *vt2*. Although deeper branches in this clade were not strongly supported (clade credibility [CC] ≥ 0.95), the seed plant, flowering plant, and monocot subclades were all strongly supported (1.00 CC). The second clade also comprised liverwort, moss, gymnosperm, and flowering plant sequences (including *Arabidopsis* TAR3 and TAR4), but only the monocot subclade was strongly supported.

vt2 was placed in a well-supported clade (1.00 CC) composed of grass species from both the BEP (*Brachypodium*, *Hordeum*, *Oryza*, *Phyllostachys*, and *Triticum*) and PACCMAD (*Setaria*, *Sorghum*, *Saccharum*, and *Zea*) clades, suggesting an origin for the *vt2/vt2-like* clade at least near the base of the grass family and possibly deeper within monocots (Figure 6). *vt2* was sister to a clade of andropogonoid sequences comprising maize *Zm2G066345* (*vt2-like*), *Sorghum* Sb03g004570, and *Saccharum* SoPUT157a-57216, and this clade was in turn sister to a *vt2-like* sequence from *Setaria italica*, suggesting that the maize *vt2* and andropogonoid *vt2-like* sequences are products of a duplication event near the base of the andropogonoid clade. In agreement with this interpretation, filtering the 15,000 optimal Bayesian trees with a constraint tree where the maize *vt2* and *vt2-like* (*Zm2G066345*) are sister taxa yielded only 73 trees or a probability of only 0.49% (73/15000) that the maize *vt2* and *vt2-like* sequences are products of the maize tetraploidy event.

The placement of *vt2* in a grass (likely monocot)-specific clade that is sister to a eudicot clade containing TAA1, TAR1, and TAR2 from *Arabidopsis* indicates that *vt2* and *vt2-like* genes from maize are co-orthologous to TAA1, TAR1, and TAR2 from *Arabidopsis*.

vt2 Is Expressed in the Epidermis and Vasculature

Sequence alignment of *vt2* with its closest homologs in maize allowed the design of gene-specific primers. RT-PCR confirmed the intron-exon boundaries predicted in *vt2* and revealed that *vt2* was broadly expressed, with expression detected in all tissues tested (Figure 7A). RNA in situ hybridization with an antisense probe to *vt2* was performed on immature tassel and ear inflorescences to determine the cell-type specificity of expression. Similar to TAA1 (Stepanova et al., 2008; Tao et al., 2008; Yamada et al., 2009), *vt2* expression was detected in the epidermis of axillary meristems and in the vasculature in the inflorescence stem (Figures 7B to 7E). *vt2* expression was first detected in the epidermis on the flanks of the

(C) Sequence alignment of the predicted *vt2* protein and three *Arabidopsis* Trp aminotransferases. *vt2* shows the highest similarity to TAR2. Asterisks indicate the position of mutations in each EMS allele. Bar line indicates the position of the *vt2-ref* deletion.

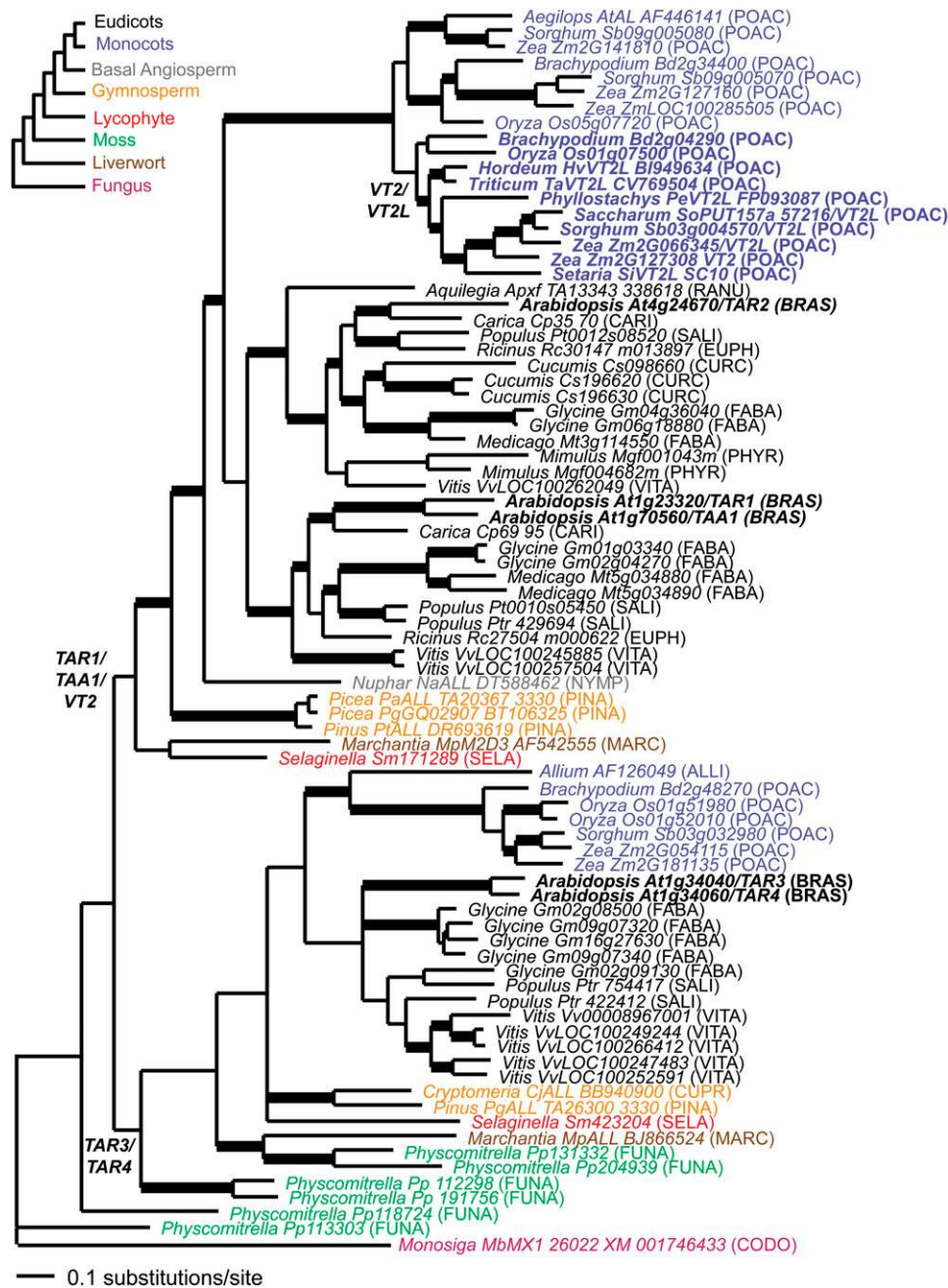


Figure 6. Phylogenetic Analysis.

Bayesian consensus phylogram of 82 *vt2*-like alliinases using the GTR model of evolution with some invariant sites and Γ distributed rates (GTR + I + Γ). Bold branches are supported by clade credibility ≥ 0.95 . Color coding depicts different taxa. The cartoon depicts the accepted relationships among sampled taxa. Family abbreviations are included in parentheses (ALLI, Alliaceae; BRAS, Brassicaceae; CARI, Caricaceae; CODO, Codonosigidae; CUPR, Cupressaceae; CURC, Cucurbitaceae; EUPH, Euphorbiaceae; FABA, Fabaceae; FUNA, Funariaceae; MARC, Marchantiaceae; NYMP, Nymphaeaceae; PHYR, Phymaceae; PINA, Pinaceae; POAC, Poaceae; RANU, Ranunculaceae; SALI, Salicaceae; SELA, Selaginaceae; SOLA, Solanaceae; and VITA, Vitaceae). The alignment used for this analysis is available as Supplemental Data Set 1 online.

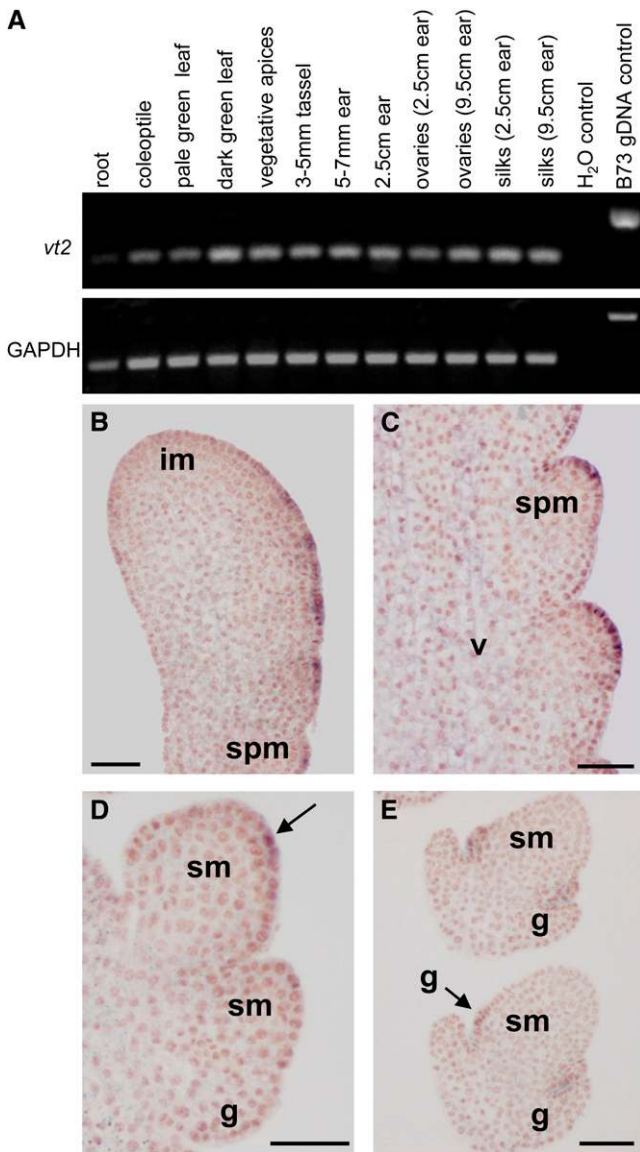


Figure 7. *vt2* Is Expressed in the Epidermis and Vasculature.

(A) Qualitative RT-PCR shows that *vt2* is expressed in all tissues tested. **(B)** to **(E)** RNA in situ hybridization on immature B73 tassels using pooled antisense probes from the 5' and 3' ends of *vt2*. im, inflorescence meristem; g, glume; v, vasculature; GAPDH, glyceraldehyde 3-phosphate dehydrogenase control. Bars = 50 μ m.

(B) Apical inflorescence meristem (from the top of a branch) showing *vt2* expression in the epidermis along the flanks of the inflorescence.

(C) Longitudinal section showing *vt2* expression in the epidermis of SPM. Weak signal is also detected in the vasculature within the inflorescence.

(D) Transverse section showing two SM. The arrow indicates *vt2* expression in the epidermis of the SM.

(E) Longitudinal section showing SM in the process of producing the outer and inner glumes. The arrow indicates *vt2* expression in the epidermis of the inner glume.

[See online article for color version of this figure.]

inflorescence meristem prior to SPM initiation (Figure 7B). As the SPM initiated, *vt2* was expressed in the epidermis in the most apical dome of the SPM (Figure 7C). As the SPM produced two SM, *vt2* was expressed in the epidermis of both SM. As meristems gave rise to lateral organs, *vt2* was again expressed in the epidermis as organs initiated (Figure 7E). We did not detect any signal using sense probes on similarly staged and treated tissues (see Supplemental Figure 2 online). Therefore, *vt2*, like *TAA1* in *Arabidopsis*, is expressed in epidermal and vascular tissue in the inflorescence (Stepanova et al., 2008; Tao et al., 2008; Yamada et al., 2009). In contrast, another gene family member, *Zm-TAR1* (Zm2g127160 in Figure 6), was recently reported to be specifically expressed in the endosperm in maize (Chourey et al., 2010).

vt2 spi1 Double Mutants Have a Slightly More Severe Phenotype Than *vt2* Single Mutants

In *Arabidopsis*, the knockout of multiple *YUC* or *TAA* genes is required to produce a severe morphological phenotype (Cheng et al., 2006, 2007a; Stepanova et al., 2008). Therefore, the effect of eliminating these two proposed pathways of Trp-dependent auxin biosynthesis has not yet been examined. As a single mutant knockout of either *spi1* or *vt2* causes a significant phenotype on its own, we constructed double mutants to determine if these two genes have overlapping functions.

spi1 mutants are slightly shorter and produce one or two fewer leaves than the wild type, hence the overall vegetative phenotype is not nearly as severe as that of *vt2* mutants (Figures 8A to 8C) (Gallavotti et al., 2008b). *vt2 spi1* double mutants revealed a vegetative phenotype very similar to that of *vt2* alone (Figure 8A). However, quantitative analysis revealed a small but statistically significant reduction in plant height (Figure 8B) and leaf number (Figure 8C) in double mutants compared with *vt2* alone.

The tassel inflorescence phenotype of *spi1* mutants is less severe than that of *vt2* mutants, with nonetheless a strong reduction in branch and functional spikelet number compared with normal (Figure 8D) (Gallavotti et al., 2008b). *vt2 spi1* double mutant tassels resembled those of *vt2* single mutants (Figure 8D), with the complete absence of branches (Figure 8G) or spikelets (Figure 8H). However, tassel length was found to be statistically significantly reduced compared with either single mutant (Figure 8F). In the female inflorescence, *spi1* mutant ears resemble *vt2* ears but are typically much less severely affected (Figure 8E). By contrast, *vt2 spi1* double mutant ears revealed a phenotype that was slightly more severe than that of *vt2* (Figure 8E). Quantification revealed a small but statistically significant reduction of ear length (Figure 8I) and kernel number (Figure 8J) in double mutants compared with *vt2*. Since double mutants could produce some ears, we also tested whether they produced an altered number of visible ear shoots. Quantification revealed that *vt2 spi1* plants produced an equivalent number of ear shoots as *vt2* plants, whereas *spi1* plants produced a similar number as wild-type plants (Figure 8K).

Although the vegetative and reproductive phenotypes initially appeared to indicate that *vt2 spi1* was similar to *vt2*, quantification revealed that *vt2 spi1* double mutants had a slightly more severe phenotype than *vt2* with respect to vegetative phenotypes and inflorescence length.

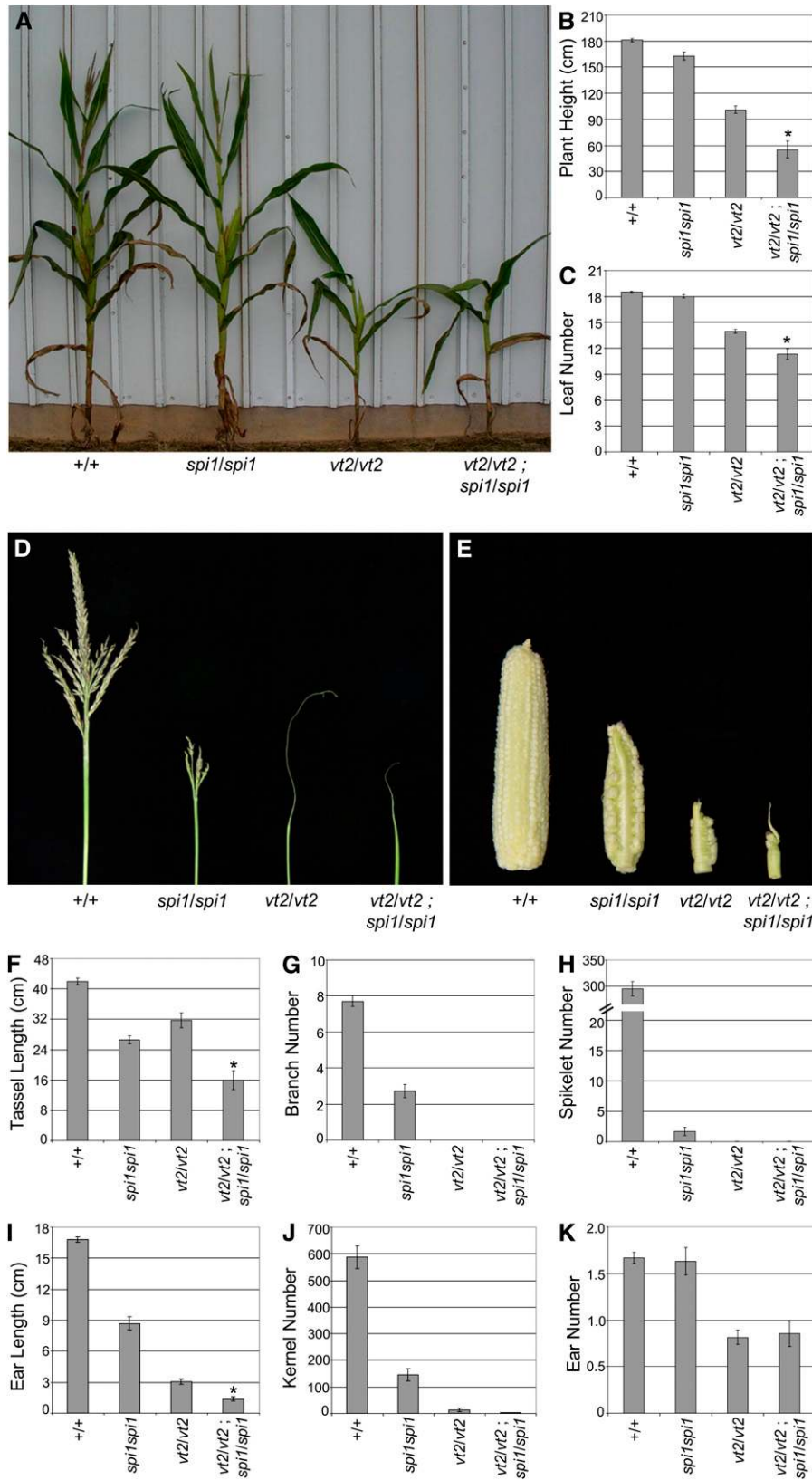


Figure 8. *vt2 spi1* Double Mutant Analysis.

Auxin Levels in Single and Double Mutants

To investigate further the functions of *spi1* and *vt2* in the biosynthesis of auxin, free IAA levels were measured (Barkawi et al., 2010). These experiments were performed in developing leaves due to the difficulties of normalizing auxin levels in developing inflorescence meristems with such dramatic morphological defects (Skirpan et al., 2009). Normal leaves had ~10 to 11 ng/g fresh weight of IAA, while *spi1* and *vt2* mutants had an average 82 and 34% of normal IAA levels, respectively (Figure 9). Surprisingly, the reduction in IAA in *spi1 vt2* double mutants was not statistically significantly different from the levels detected in *vt2* single mutants (P value = 0.845). These results provide experimental support for the hypothesis that *vt2* and *spi1* may actually function in the same pathway for auxin biosynthesis, at least in leaf tissue.

vt2 and *bif2* Exhibit a Synergistic Interaction

The effects of eliminating both a gene in auxin biosynthesis and a gene in auxin transport have been examined in maize through double mutant combinations with *spi1* and *bif2* (Gallavotti et al., 2008b). The results of those studies revealed a synergistic interaction that produced double mutant plants with a very similar vegetative phenotype to that of *vt2* mutants (Gallavotti et al., 2008b). To test the interaction of *vt2* and *bif2*, we constructed double mutants.

In the vegetative phase of growth, *bif2* mutants have a slight reduction in plant height and leaf number compared with wild-type plants (Figures 10A to 10C) (McSteen et al., 2007). By contrast, the *vt2 bif2* double mutant vegetative phenotype was extremely severe (Figure 10A, inset). Double mutants exhibited a significant reduction in plant height to ~10% of normal (Figure 10B) and significantly fewer leaves with only about seven total leaves produced (Figure 10C). In fact, the phenotype was so severe that double mutants died weeks before siblings flowered.

bif2 single mutants typically produce tassels with a reduced number of branches, spikelets, florets, and floral organs (Figure 10D) (McSteen and Hake, 2001). *vt2 bif2* double mutants produced completely barren tassels similar to *vt2* single mutants, although they also had an extreme reduction in size (Figure 10D).

Quantification of tassel length confirmed a significant reduction in *vt2 bif2* mutants compared with either single mutant alone (Figure 10E). In addition, *vt2 bif2* mutants never produced visible ear shoots, which is a more severe phenotype than either single mutant (Figure 10F).

Both vegetative and reproductive data for *vt2 bif2* double mutants show a phenotype that is significantly more severe than either single mutant alone. This can be interpreted as a synergistic interaction, indicating that *vt2* and *bif2* have overlapping functions in vegetative and reproductive development in maize.

vt2 Is Epistatic to *ba1*

To investigate the interaction of *vt2* with another barren inflorescence mutant that does not have defects in auxin transport or biosynthesis, we constructed double mutants with *barren stalk1* (*ba1*), which has defects in the production of all axillary meristems (Ritter et al., 2002; Gallavotti et al., 2008a). *ba1* mutants do not show an obvious vegetative phenotype except for a reduction in height (see Supplemental Figures 3A and 3B online), which is due to a decrease in tassel length (see Supplemental Figure 3E online), rather than leaf number (see Supplemental Figure 3C online). The *vt2 ba1* double mutant vegetative phenotype clearly resembled that of *vt2* single mutants (see Supplemental Figure 3A online). Quantification revealed that there was no statistically significant reduction in plant height (see Supplemental Figure 3B online) or leaf number (see Supplemental Figure 3C online) in *vt2 ba1* double mutants compared with *vt2* alone.

ba1 mutants produce tassel inflorescences similar to those of *vt2* mutants, exhibiting a complete lack of branches and spikelets (see Supplemental Figure 3D online). However, unlike *vt2* mutants, *ba1* tassels produce suppressed bract primordia (visible as bumps) in regular rows along the rachis of the tassel (see Supplemental Figure 3D online, arrow) (Ritter et al., 2002). These bumps indicate pools of auxin that are produced and transported normally to the inflorescence but cannot be used to produce spikelets due to the absence of *ba1* gene function (Gallavotti et al., 2008a). *vt2 ba1* double mutants produced tassels that resembled *vt2* single mutants, with no evidence of bract primordia that are normally observed in *ba1* single mutants (see Supplemental Figure 3D online). Tassel length of *vt2 ba1* double mutants

Figure 8. (continued).

(A) *vt2 spi1* plants resemble *vt2* single mutants except with a reduction in height.

(B) Quantification of plant height.

(C) Quantification of leaf number.

(D) *vt2 spi1* tassels resemble *vt2* single mutants except with a reduction in length.

(E) *vt2 spi1* ears exhibit reduced length and kernel number.

(F) Quantification of tassel length.

(G) Quantification of tassel branch number.

(H) Quantification of tassel spikelet number.

(I) Quantification of ear length.

(J) Quantification of kernel number.

(K) Quantification of visible ear shoot number. Asterisk indicates significant reduction at $P < 0.05$ compared with either single mutant alone; error bars represent the SE; $n = 55$ normal, 17 *spi1*, 27 *vt2*, 7 *vt2 spi1* for (B), (C), and (K); $n = 10$ normal, *spi1*, and *vt2* and 7 *vt2 spi1* for (F) to (H); $n = 5$ each of normal, *spi1*, *vt2*, and *vt2 spi1* for (I) and (J).

[See online article for color version of this figure.]

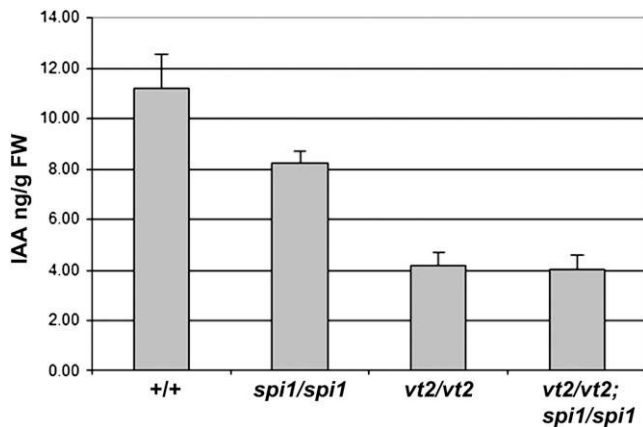


Figure 9. Measurement of Free IAA Levels in Normal, *spi1*, *vt2*, and *spi1 vt2* Mutants.

Free IAA levels were measured in developing leaves of 2-week-old seedlings. Error bars represent the SE. $n = 5$ each of normal, *spi1*, *vt2*, and *vt2 spi1*. One replicate of three is shown. FW, fresh weight.

was not significantly different than either single mutant alone (see Supplemental Figure 3E online). Finally, *ba1* mutants never produce ears since they lack the ability to initiate ear axillary meristems, and *vt2 ba1* double mutants similarly never produced an ear shoot (see Supplemental Figure 3F online).

These results illustrate that *vt2* is completely epistatic to *ba1* during both vegetative and tassel inflorescence development. As *ba1* mutants do not produce ear shoots, *ba1* is epistatic to *vt2* during the production of the ear. These results support the idea that *vt2* is functioning upstream in auxin production, while *ba1* is functioning downstream in the production of axillary meristems.

DISCUSSION

Here, we show that the *vt2* plays a significant role in axillary meristem formation during inflorescence development in maize. During vegetative development, *vt2* does not play a role in axillary meristem formation but functions in leaf initiation during the adult phase of growth. *vt2* encodes an enzyme with similarity to TAA1, which has been demonstrated to convert Trp to IPA in *Arabidopsis* (Stepanova et al., 2008; Tao et al., 2008; Yamada et al., 2009). Phylogenetic analysis indicates that *vt2* is co-orthologous to TAA1, TAR1, and TAR2 in *Arabidopsis*. Our results suggest that the IPA pathway for Trp-dependent auxin biosynthesis contributes significantly to vegetative and reproductive development in maize.

Auxin Biosynthesis Pathways in Maize and *Arabidopsis*

The phenotype of *vt2* mutants shares many similarities with the phenotype of *spi1* mutants, which are defective in the proposed TAM pathway for Trp-dependent auxin biosynthesis in maize (Gallavotti et al., 2008b). Both mutants have defects in axillary meristem formation during reproductive development, shorter inflorescences due to defects in cell elongation, and shorter plant height due to defects in leaf initiation during vegetative development

(Gallavotti et al., 2008b; Barazesh et al., 2009). The *vt2* mutant, however, has more severe defects than does *spi1*, although both are presumed to be null alleles. The similarity in phenotype is not due to effects on gene expression as real-time RT-PCR experiments indicate that *spi1* expression is not reduced in *vt2* mutants nor is *vt2* expression reduced in *spi1* mutants (see Supplemental Figure 4 online). Both *spi1* and *vt2* mutants have reduced free auxin levels, indicating that both gene products contribute to the production of auxin in the plant. In *Arabidopsis*, the similarity of phenotype of *yuc* and *taa* multiple mutant combinations has been used as an argument to suggest that these two genes act in the same pathway for the production of auxin rather than being separate independent pathways (Strader and Bartel, 2008).

In *Arabidopsis*, multiple knockouts of the TAA genes or the YUC genes are required to produce a severe phenotype, whereas in maize, single knockouts of either *vt2* or *spi1* have a dramatic effect on development (Cheng et al., 2006, 2007a; Gallavotti et al., 2008b; Stepanova et al., 2008). The availability of single gene knockouts with dramatic phenotypes in maize enabled us to test the relative contribution of the *vt2* and *spi1* genes to development through the construction of double mutants. The results show that *vt2 spi1* double mutants have a slightly more severe phenotype than the *vt2* single mutant does. This interaction could be interpreted as additive, although synergism, epistasis, and additivity can be difficult to distinguish when mutants have similar phenotypes. When both mutants are null, an additive interaction is interpreted to indicate that the genes function in different pathways. However, when mutants are not null, a more severe phenotype in the double mutant is interpreted to indicate that the genes function in the same pathway (Martienssen and Irish, 1999). The presence of other *spi1* and *vt2* gene family members expressed during vegetative and reproductive development (K.A. Phillips and P. McSteen, unpublished data) suggests that the function of the gene family has not been completely knocked out in the single mutants. Therefore, the more severe phenotype in the *vt2 spi1* double mutant could also be interpreted to imply that the *spi1* and *vt2* genes function in the same pathway. Although the genetic interaction could be interpreted to support either hypothesis, the observation that the double mutant does not have a statistically significant reduction in auxin levels compared with the *vt2* single mutant provides some support for the hypothesis that the two genes may act in the same pathway. However, the alternative hypothesis that they act in different pathways has not been disproven by these results as auxin levels rather than auxin biosynthetic rates were measured. Therefore, further analysis of the in vivo functions of these enzymes is essential.

The hypothesis of multiple auxin biosynthetic pathways also raises the question of why the different pathways do not compensate for each other in either maize or *Arabidopsis* (Tao et al., 2008). This lack of compensation has been used as an argument to support the hypothesis that the YUC and TAA genes may act in the same pathway (Strader and Bartel, 2008). In fact, in *Arabidopsis*, upregulation of the IAOx pathway has been shown to compensate for defects in the IPA pathway (Stepanova et al., 2008), and expression of the bacterial *iaaM* gene, which catalyzes the conversion of Trp to IAM, can rescue the *yuc1 yuc4* double mutant in *Arabidopsis* (Cheng et al., 2006). Therefore, when misregulated, other auxin biosynthetic pathways can compensate for deficiencies in the TAM or IPA pathways in *Arabidopsis*. This

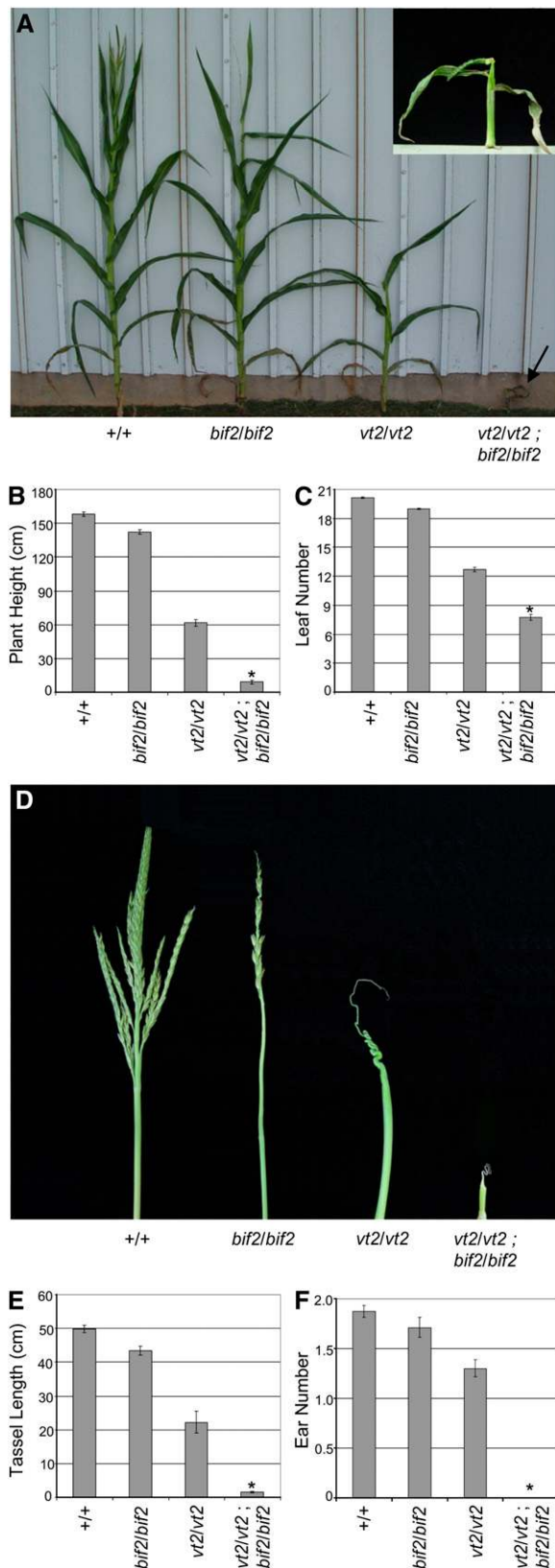


Figure 10. *vt2 bif2* Double Mutant Analysis.

indicates that lack of compensation may be due to differences in expression pattern or availability of intermediates in different cell types. *spi1* and *vt2* are both expressed as axillary meristems and lateral organs initiate in the inflorescence, although *spi1* expression extends several cell layers instead of being restricted to the epidermis as for *vt2* (Gallavotti et al., 2008b); therefore, lack of compensation by the two proposed pathways in maize cannot wholly be explained by differences in expression pattern. The identification of *spi1* and *vt2* gene family members specifically expressed in the endosperm of maize suggests that these enzyme activities may also overlap during endosperm development (Chourey et al., 2010; LeClere et al., 2010). Moreover, the recent findings questioning the biochemical function of YUC indicate that much remains to be learned about how these pathways function (Tivendale et al., 2010; Nonhebel et al., 2011). Much also remains to be learned about the differences in auxin biosynthesis pathways in different plant species and in different tissues (Quittenden et al., 2009; Ishii et al., 2010; Tivendale et al., 2010).

In contrast with the similarity in phenotype seen between *vt2* and *spi1* mutants, *vt2* mutants have few similarities with the phenotypes of *taa1*, *tar1*, and *tar2* single, double, and triple mutants in *Arabidopsis* (Stepanova et al., 2008). Some of these differences may be superficial due to the fact that, for example, leaf and flower number have not been quantified in *taa1 tar* double mutants, and *vt2* mutants have similarly not been tested for insensitivity to ethylene, shade, or naphthylphthalamic acid. One clear difference between maize and *Arabidopsis* is that the *Arabidopsis taa1 tar2* double mutants have very significant defects in apical dominance, exhibiting a bushy phenotype presumably due to outgrowth of secondary branches. By contrast, bushiness is not a characteristic of the maize *vt2* mutants. In fact, testing the interaction of *vt2* with *tb1* showed that *vt2* did not appear to play a role in suppression or promotion of axillary branch outgrowth. These apparent differences between *vt2* and *taa1* mutants could be due to roles of additional gene family members that have not yet been fully addressed in either maize or *Arabidopsis*.

The Role of Temperature in Auxin Biosynthesis

Another point of contrast between *vt2* and *taa1* mutants is that both exhibit temperature dependence but they have opposite responses to high temperature. Maize *vt2* mutants have a weaker inflorescence phenotype at high temperature, whereas some defects in

(A) *vt2 bif2* plants (arrow and inset) exhibit a drastic reduction in vegetative growth compared with *vt2* or *bif2* single mutants.

(B) Quantification of plant height.

(C) Quantification of leaf number.

(D) *vt2 bif2* tassels are severely underdeveloped compared with *vt2* or *bif2* single mutants.

(E) Quantification of tassel length.

(F) Quantification of ear number. Asterisk indicates significant reduction at $P < 0.05$ compared with either single mutant alone; error bars represent the SE; $n = 31$ normal, 28 *bif2*, 18 *vt2*, and 6 *vt2 bif2* for **(B)**, **(C)**, and **(F)**; $n = 10$ normal, *bif2*, and *vt2* and 8 *vt2 bif2* for **(E)**.

[See online article for color version of this figure.]

Arabidopsis *taa1* mutants can be detected only at high temperature (Yamada et al., 2009). It has been shown in *Arabidopsis* that free auxin levels in hypocotyls increase at higher temperature (Gray et al., 1998), and it now appears that multiple auxin biosynthetic pathways may be contributing to these increased levels. The *TAA1* gene is temperature induced, and temperature-induced hypocotyl elongation is abolished in *taa1* mutants, indicating that the IPA pathway is induced by high temperature in *Arabidopsis* (Yamada et al., 2009). Furthermore, in the IAOx pathway, *Arabidopsis* *cyp79b2 cyp79b3* double mutants were shown to have reduced auxin levels at higher temperature compared with the wild type, indicating that the IAOx pathway also contributes to increased auxin levels at higher temperatures (Zhao et al., 2002). As the IAOx pathway is not supposed to be critical outside the Brassicaceae (Sugawara et al., 2009), one possible explanation for the weaker phenotype of maize *vt2* mutants at higher temperature is that closely related *vt2-like* genes may be capable of providing increased activity at high temperatures. Alternately, *spi1* may contribute to auxin biosynthesis at higher temperature, as the *spi1* mutant does not have a weaker phenotype at higher temperature. However, *YUC* gene expression has been shown to be reduced rather than increased in anthers of barley (*Hordeum vulgare*) and *Arabidopsis* at high temperature (Sakata et al., 2010). Therefore, future work is required to address the role of all gene family members and their relative contributions to auxin biosynthesis at different temperatures, in different tissues, and in different species.

Synergistic Interaction of Auxin Biosynthesis and Auxin Transport

In contrast with the slightly enhanced phenotype observed in *vt2 spi1* double mutants, synergistic interactions are seen when both auxin biosynthesis and auxin transport are reduced. This was demonstrated in *spi1 bif2* double mutants, as disruption of each single gene has mild effects on vegetative development, but dramatic effects are observed in the double mutant combination (Gallavotti et al., 2008b). *vt2 bif2* double mutants show even more dramatic effects on plant height and leaf number, causing the plants to complete development and senesce weeks earlier than normal. These synergistic interactions indicate that both auxin transport and biosynthesis play overlapping roles in normal development. Synergistic interactions between auxin biosynthesis and transport have previously been reported in *Arabidopsis*, indicating that this phenomenon is widespread (Weijers et al., 2005; Cheng et al., 2007a, 2007b). Furthermore, it has been shown in *Arabidopsis* that auxin synthesized by *TAA1* in the leaves has to be transported to the stem to exert its effects (Tao et al., 2008). Therefore, both auxin transport and auxin biosynthesis play critical roles in vegetative and reproductive development.

METHODS

Origin of *vt2* Alleles

The *vt2-ref* allele originated by *Mu* transposon mutagenesis (Smith and Hake, 1993). *vt2-TR799*, *vt2-GN21*, *vt2-GN210*, and *vt2-GN327* were obtained from the Maize Inflorescence Project and arose via EMS mutagenesis in defined genetic backgrounds (<http://www.maizegdb.org>).

vt2-RM123 was obtained from the *RescueMu* population (<http://www.maizegdb.org/rescuemu-phenotype.php>). *vt2-DB1845* arose by spontaneous mutation in the maize (*Zea mays*) B73 genetic background (David Braun, Penn State University).

Mature Phenotype Analysis

All mature phenotype data were obtained using the *vt2-ref* allele backcrossed into the B73 background six times and compared with normal siblings from the same family. Segregating families were planted in two separate field plantings during the summer in Rocksprings, PA, grown to maturity (10 to 12 weeks), and scored for phenotype. Data presented are representative of one field season. Plant height was obtained by measuring from the ground to the tip of the tassel, and ear number was scored by counting all visible ears on each plant. Leaf number was quantified by marking every 5th leaf of developing field-grown plants beginning at 4 weeks until full maturity. Tassel length was calculated by measuring from the tip of the tassel to the base of the flag leaf node, and branch number was obtained by counting all visible lateral branches. Spikelet number was obtained prior to anthesis by removing and counting all spikelets from the branches and main spike. Kernel number was estimated by counting all spikelets on mature open-pollinated ears, and ear length was obtained by measuring these ears from the base to the tip.

For leaf juvenile-to-adult transition analysis, segregating families were greenhouse-grown for 9 weeks and genotyped for *vt2* using a TaqMan SNP assay (described below). Leaf number was counted as described above. As leaves fully emerged from the whorl, the presence or absence of epicuticular waxes on the blade was evaluated for leaves 1 to 10.

For double mutant analysis, segregating families were planted twice separated by a few weeks and grown to maturity (10 to 12 weeks) in Rocksprings, PA in the summer of 2007 and 2008 (2008 and 2009 for *vt2 spi1*). Similar results were also seen in Columbia, MO in the summer of 2010. Data shown are representative of one planting from the 2008 field season except for the ear data from *vt2 spi1* double mutants, which are from the 2009 field season. *vt2 tb1* double mutant families were generated using the *tb1-ref* allele (Doebley et al., 1997) in the B73 background. Visible tillers were counted at maturity as those that were derived directly from one of the nodes on the main stalk. *vt2 spi1* double mutant families were generated using the *spi1-ref* allele (Gallavotti et al., 2008b) in the B73 background. All individuals were genotyped for *vt2* using the SNP TaqMan protocol and for *spi1* as previously described (Gallavotti et al., 2008b). *vt2 bif2* double mutant families were generated using the *bif2-77* allele (McSteen et al., 2007) in the B73 background. All individuals were genotyped for *vt2* using the SNP TaqMan protocol and for *bif2* as previously described (Skirpan et al., 2008). Data for all *vt2 bif2* double mutants were obtained about 7 weeks after germination due to the drastically reduced lifespan of the plants. Photos display younger *vt2 bif2* mutants next to siblings from a planting 2 weeks earlier to represent all individuals at maturity. *vt2 ba1* double mutant families were generated using the *ba1-ref* allele (Ritter et al., 2002) in the B73 background.

For statistical analysis, results were analyzed using Microsoft Excel 2003. Bar graphs were produced using the mean of each data set, and error bars are the SE. Data were considered statistically significant at P value < 0.05 using the Student's two-tailed t test in Microsoft Excel.

TaqMan *vt2* Genotyping Assay

The Panzea database was used to identify SNPs in the *vt2* region after preliminary fine-mapping (www.panzea.org). A SNP located on contig 327 was identified to be polymorphic between *vt2* mutants (*C_{GA}*) and the B73 background (*C_{AA}*). Primers flanking the SNP were designed based on the Panzea sequence, and the SNP was confirmed to be linked to the *vt2* mutant background by DNA sequencing. A TaqMan SNP genotyping assay (primers in Supplemental Table 3 online) was then designed using

the Custom TaqMan SNP Genotyping Assays design program, File Builder v3.1 (Applied Biosystems). TaqMan assays were performed by the Penn State Huck Institutes Genomics Core Facility using an ABI 7300 sequence detection system.

Measurement of Cell Size

For measurement of cell size, nail polish impressions were obtained from the basal region of five wild-type and *vt2* field-grown tassels at maturity as previously described (Barazesh et al., 2009). Slides were analyzed at $\times 20$ magnification using a Nikon Eclipse 80i upright microscope on the bright-field setting and a Nikon DM1200F camera. Approximately 15 to 30 cells were measured per biological replicate depending on cell size. The average lengths of each replicate were used to obtain the final mean presented for each genotype.

Scanning Electron Microscopy

Families segregating for *vt2-ref* in the B73 genetic background were planted and genotyped using the TaqMan assay. Ears were collected from field-grown plants after ~ 8 weeks, while tassels were collected from both field- and greenhouse-grown plants after ~ 5 weeks. Field-grown plants were exposed to an average daily minimum temperature of 12.9°C and an average daily maximum temperature of 23.7°C according to weather history data available for Pennsylvania Furnace, PA from May 19, 2009 through July 10, 2009 (www.almanac.com). Greenhouse temperatures in the maize growth rooms were held at a minimum temperature of 26.7°C for both day and night, with daytime temperatures typically increasing an additional 5 to 10°C. Cooler greenhouse rooms were held at a minimum temperature of 20°C and a maximum temperature of 26.7°C each day. Fixation and scanning electron microscopy of samples were performed as previously described (Wu and McSteen, 2007).

Phylogenetic Analyses

vt2-like alliinase sequences were retrieved using BLAST searches at CoGe (<http://synteny.cnr.berkeley.edu/CoGe>), the National Center for Biotechnology Information (<http://www.ncbi.nlm.nih.gov>), Phytozome (<http://www.phytozome.org>), PlantGDB (<http://www.plantgdb.org>), and The Institute for Genomic Research (http://blast.jcvi.org/euk-blast/plant-ta_blast.cgi). The resulting nucleotide sequences were then aligned using the conceptual amino acid translation using MacClade (Maddison and Maddison, 2003) and MUSCLE (Edgar, 2004) before being manually adjusted. Hypervariable regions of the alignment between nucleotide positions 1 to 567 and 2197 to 3027 were considered too divergent for reliable alignment and were excluded from subsequent analyses (see Supplemental Data Set 1 online for the alignment). Phylogenetic relationships were estimated with MrBayes 3.1 (Ronquist and Huelsenbeck, 2003) on the Grethor parallel processing cluster at the University of Missouri–St. Louis using the General Time Reversible (GTR) model of evolution with invariant sites and gamma distributed rates (GTR + I + Γ), with the nucleotide data set partitioned according to codon position. Bayesian phylogenetic analysis consisted of two separate runs of four chains of 10 million generations with trees sampled every 1000 generations and the first 25% (2500 trees) of suboptimal trees removed as burnin. Trees were rooted using a fungal Asp aminotransferase (Monosiga XM_001746433) as an outgroup. Constraint trees were generated in MacClade, and the sets of optimal trees from the Bayesian analyses were filtered using PAUP 3.1 (Swofford, 2000).

Expression Analysis

cDNA was generated from total RNA for each tissue sample using the High Capacity cDNA reverse transcription kit (Applied Biosystems). Three

μL of cDNA was amplified by PCR using the *vt2* gene-specific primers ex34-F and ex34-R (see Supplemental Table 3 online) for 40 cycles. GAPDH primers L4 and R4 (see Supplemental Table 3 online) were used as controls and amplified 1 μL of cDNA for 35 cycles. RNA in situ hybridization was performed as described (Jackson et al., 1994). The 5' antisense probe construct was amplified using primers 5'probe-F and 5'probe-R (see Supplemental Table 3 online) and cloned into the pGemTEasy vector (Promega). The 3' antisense probe construct was amplified using primers 3'probe-F and 3'probe-R (see Supplemental Table 3 online) and cloned into the pGemTEasy vector. DNA template was amplified by PCR using M13 forward and reverse primers and DIG-labeled antisense RNA probe generated with SP6 RNA polymerase. One microliter of both 5' and 3' probe was pooled prior to hybridization on slides. Sense probes were generated from the same constructs using T7 RNA polymerase. Immature greenhouse-grown B73 tassels were fixed and embedded in paraffin wax as previously described except that fixation was for ~ 2 h (Wu and McSteen, 2007). Real-time RT-PCR was performed as described (Barazesh and McSteen, 2008) using Taqman assays (probes and primers listed in Supplemental Table 3 online) and total RNA extracted from immature leaf tissue.

Quantification of Free IAA

Families segregating for both *spi1* and *vt2* in the B73 genetic background were grown for 2 weeks and genotyped as described above. Samples of leaf tissue were collected from the fifth leaf that was just emerging from the whorl. Leaf tissue (50 to 80 mg) was weighed, frozen in liquid nitrogen, and stored at -80°C . For each sample, 150 μL of homogenization buffer (35% of 0.2 M imidazole and 65% isopropanol, pH 7) containing 3 or 4 ng of [$^{13}\text{C}_6$]IAA was added before homogenization. The level of free IAA was analyzed by solid phase extraction followed by selected ion monitoring–gas chromatography–mass spectrometry as previously described (Barkawi et al., 2010).

Accession Numbers

vt2 genomic and cDNA nucleotide sequence data reported are available in the Third Party Annotation Section of the GenBank/EMBL/DDBJ databases under the accession number BK007972 (TPA). The accession numbers for sequences used in the phylogenetic analysis in Figure 6 can be found in Supplemental Table 4 online.

Supplemental Data

The following materials are available in the online version of this article.

Supplemental Figure 1. Scanning Electron Microscopy Analysis of *vt2* Ear Inflorescences.

Supplemental Figure 2. RNA in Situ Hybridization with *vt2* Sense Probes.

Supplemental Figure 3. *vt2 ba1* Double Mutant Analysis.

Supplemental Figure 4. Real-Time Expression Analysis.

Supplemental Table 1. *vt2* Juvenile-to-Adult Leaf Transition Is Not Significantly Different from Normal Siblings.

Supplemental Table 2. *vt2* Mutant Tassels Exhibit Reduced Cell Length Compared with Normal Siblings.

Supplemental Table 3. Primers Used for *vt2* Mapping, Cloning, Genotyping, and Expression Analyses.

Supplemental Table 4. Accession Numbers for Sequences Used in Phylogenetic Analysis in Figure 6.

Supplemental Data Set 1. Text File of the Alignment Used for the Phylogenetic Analysis in Figure 6.

ACKNOWLEDGMENTS

We thank Frank Baker for advice and assistance with scoring juvenile versus adult leaves. We thank W. Scott Harkom, Tony Omeis, and Tom Slewinski for plant care in the greenhouse and the field. We thank Missy Hazen and Ruth Haldeman of the Pennsylvania State University Huck Institutes Electron Microscopy facility for assistance with scanning electron microscopy and Deb Grove and Ashley Price of the Huck Institutes Genomics core facility for assistance with DNA sequencing, TaqMan genotyping, and real-time RT-PCR assays. We thank Jessica Levy and Matthew Phillips for assistance in the field and Peng Yu for assistance with auxin measurements. We also thank the University of Missouri–St. Louis for access to their Grethor parallel-processing cluster and Elizabeth Kellogg (University of Missouri–St. Louis), Jeff Bennetzen and Ryan Percifield (University of Georgia), and the Joint Genome Institute for providing the *Setaria italica* vt2 genomic sequence. This research was supported by USDA Grant 2007-03036 to P.M., National Science Foundation Grant IOS-0820729 to P.M. and S.M., and National Science Foundation Grants MCB0725149 and IOS-PGRP-0923960 and the Gordon and Margaret Bailey Endowment for Environmental Horticulture to J.D.C.

Received March 11, 2010; revised January 4, 2011; accepted January 27, 2011; published February 18, 2011.

REFERENCES

- Barazesh, S., and McSteen, P.** (2008). *Barren inflorescence1* functions in organogenesis during vegetative and inflorescence development in maize. *Genetics* **179**: 389–401.
- Barazesh, S., Nowbakt, C., and McSteen, P.** (2009). *sparse inflorescence1*, *barren inflorescence1* and *barren stalk1* promote cell elongation in maize inflorescence development. *Genetics* **182**: 403–406.
- Barkawi, L.S., Tam, Y.Y., Tillman, J.A., Normanly, J., and Cohen, J.D.** (2010). A high-throughput method for the quantitative analysis of auxins. *Nat. Protoc.* **5**: 1609–1618.
- Bartel, B.** (1997). Auxin biosynthesis. *Annu. Rev. Plant Physiol.* **48**: 49–64.
- Bartling, D., Seedorf, M., Mithöfer, A., and Weiler, E.W.** (1992). Cloning and expression of an Arabidopsis nitrilase which can convert indole-3-acetonitrile to the plant hormone, indole-3-acetic acid. *Eur. J. Biochem.* **205**: 417–424.
- Benjamins, R., and Scheres, B.** (2008). Auxin: The looping star in plant development. *Annu. Rev. Plant Biol.* **59**: 443–465.
- Bennett, S.R.M., Alvarez, J., Bossinger, G., and Smyth, D.R.** (1995). Morphogenesis in *pinoid* mutants of *Arabidopsis thaliana*. *Plant J.* **8**: 505–520.
- Chandler, J.W.** (2009). Local auxin production: A small contribution to a big field. *Bioessays* **31**: 60–70.
- Cheng, P.C., Greyson, R.I., and Walden, D.B.** (1983). Organ initiation and the development of unisexual flowers in the tassel and ear of *Zea mays*. *Am. J. Bot.* **70**: 450–462.
- Cheng, Y., Dai, X., and Zhao, Y.** (2007a). Auxin synthesized by the YUCCA flavin monooxygenases is essential for embryogenesis and leaf formation in *Arabidopsis*. *Plant Cell* **19**: 2430–2439.
- Cheng, Y., Qin, G., Dai, X., and Zhao, Y.** (2007b). NPY1, a BTB-NPH3-like protein, plays a critical role in auxin-regulated organogenesis in *Arabidopsis*. *Proc. Natl. Acad. Sci. USA* **104**: 18825–18829.
- Cheng, Y.F., Dai, X.H., and Zhao, Y.D.** (2006). Auxin biosynthesis by the YUCCA flavin monooxygenases controls the formation of floral organs and vascular tissues in *Arabidopsis*. *Genes Dev.* **20**: 1790–1799.
- Chourey, P.S., Li, Q.-B., and Kumar, D.** (2010). Sugar-hormone cross-talk in seed development: two redundant pathways of IAA biosynthesis are regulated differentially in the invertase-deficient *miniature1* (*mn1*) seed mutant in maize. *Mol. Plant* **3**: 1026–1036.
- Christensen, S.K., Dagenais, N., Chory, J., and Weigel, D.** (2000). Regulation of auxin response by the protein kinase PINOID. *Cell* **100**: 469–478.
- Doebley, J., Stec, A., and Hubbard, L.** (1997). The evolution of apical dominance in maize. *Nature* **386**: 485–488.
- Edgar, R.C.** (2004). MUSCLE: A multiple sequence alignment method with reduced time and space complexity. *BMC Bioinformatics* **5**: 113.
- Friml, J., et al.** (2004). A PINOID-dependent binary switch in apical-basal PIN polar targeting directs auxin efflux. *Science* **306**: 862–865.
- Gallavotti, A., Barazesh, S., Malcomber, S., Hall, D., Jackson, D., Schmidt, R.J., and McSteen, P.** (2008b). *sparse inflorescence1* encodes a monocot-specific YUCCA-like gene required for vegetative and reproductive development in maize. *Proc. Natl. Acad. Sci. USA* **105**: 15196–15201.
- Gallavotti, A., Yang, Y., Schmidt, R.J., and Jackson, D.** (2008a). The relationship between auxin transport and maize branching. *Plant Physiol.* **147**: 1913–1923.
- Gälweiler, L., Guan, C.H., Müller, A., Wisman, E., Mendgen, K., Yephremov, A., and Palme, K.** (1998). Regulation of polar auxin transport by AtPIN1 in Arabidopsis vascular tissue. *Science* **282**: 2226–2230.
- Gray, W.M., Ostin, A., Sandberg, G., Romano, C.P., and Estelle, M.** (1998). High temperature promotes auxin-mediated hypocotyl elongation in Arabidopsis. *Proc. Natl. Acad. Sci. USA* **95**: 7197–7202.
- Hubbard, L., McSteen, P., Doebley, J., and Hake, S.** (2002). Expression patterns and mutant phenotype of *teosinte branched1* correlate with growth suppression in maize and teosinte. *Genetics* **162**: 1927–1935.
- Ishii, T., Soeno, K., Asami, T., Fujioka, S., and Shimada, Y.** (2010). Arabidopsis seedlings over-accumulated indole-3-acetic acid in response to aminooxyacetic acid. *Biosci. Biotechnol. Biochem.* **74**: 2345–2347.
- Jackson, D., Veit, B., and Hake, S.** (1994). Expression of maize *knotted1* related homeobox genes in the shoot apical meristem predicts patterns of morphogenesis in the vegetative shoot. *Development* **120**: 405–413.
- Kerstetter, R.A., and Poethig, R.S.** (1998). The specification of leaf identity during shoot development. *Annu. Rev. Cell Dev. Biol.* **14**: 373–398.
- Kleine-Vehn, J., Huang, F., Naramoto, S., Zhang, J., Michniewicz, M., Offringa, R., and Friml, J.** (2009). PIN auxin efflux carrier polarity is regulated by PINOID kinase-mediated recruitment into GNOM-independent trafficking in *Arabidopsis*. *Plant Cell* **21**: 3839–3849.
- Kriechbaumer, V., Park, W.J., Gierl, A., and Glawischnig, E.** (2006). Auxin biosynthesis in maize. *Plant Biol (Stuttg)* **8**: 334–339.
- Kriechbaumer, V., Park, W.J., Piotrowski, M., Meeley, R.B., Gierl, A., and Glawischnig, E.** (2007). Maize nitrilases have a dual role in auxin homeostasis and beta-cyanoalanine hydrolysis. *J. Exp. Bot.* **58**: 4225–4233.
- Kriechbaumer, V., Weigang, L., Fiesselmann, A., Letzel, T., Frey, M., Gierl, A., and Glawischnig, E.** (2008). Characterisation of the tryptophan synthase alpha subunit in maize. *BMC Plant Biol.* **8**: 44.
- Kuettner, E.B., Hilgenfeld, R., and Weiss, M.S.** (2002). The active principle of garlic at atomic resolution. *J. Biol. Chem.* **277**: 46402–46407.
- LeClere, S., Schmelz, E.A., and Chourey, P.S.** (2010). Sugar levels regulate tryptophan-dependent auxin biosynthesis in developing maize kernels. *Plant Physiol.* **153**: 306–318.
- Lehmann, T., Hoffmann, M., Hentrich, M., and Pollmann, S.** (2010).

- Indole-3-acetamide-dependent auxin biosynthesis: a widely distributed way of indole-3-acetic acid production? *Eur. J. Cell Biol.* **89**: 895–905.
- Maddison, D.R., and Maddison, W.P.** (2003). *MacClade: Analysis of Phylogeny and Character Evolution*. (Sunderland, MA: Sinauer Associates).
- Martienssen, R., and Irish, V.** (1999). Copying out our ABCs: The role of gene redundancy in interpreting genetic hierarchies. *Trends Genet.* **15**: 435–437.
- McSteen, P.** (2010). Auxin and monocot development. *Cold Spring Harb. Perspect. Biol.* **2**: a001479.
- McSteen, P., and Hake, S.** (2001). *barren inflorescence2* regulates axillary meristem development in the maize inflorescence. *Development* **128**: 2881–2891.
- McSteen, P., Laudencia-Chingcuanco, D., and Colasanti, J.** (2000). A floret by any other name: control of meristem identity in maize. *Trends Plant Sci.* **5**: 61–66.
- McSteen, P., Malcomber, S., Skirpan, A., Lunde, C., Wu, X., Kellogg, E., and Hake, S.** (2007). *barren inflorescence2* Encodes a co-ortholog of the *PINOID* serine/threonine kinase and is required for organogenesis during inflorescence and vegetative development in maize. *Plant Physiol.* **144**: 1000–1011.
- Nonhebel, H., Yuan, Y., Al-Amier, H., Pieck, M., Akor, E., Ahamed, A., Cohen, J.D., Celenza, J.L., and Normanly, J.** (2011). Redirection of tryptophan metabolism in tobacco by ectopic expression of an Arabidopsis indolic glucosinolate biosynthetic gene. *Phytochemistry* **72**: 37–48.
- Park, W.J., Kriechbaumer, V., Möller, A., Piotrowski, M., Meeley, R.B., Gierl, A., and Glawischnig, E.** (2003). The nitrilase *ZmNIT2* converts indole-3-acetonitrile to indole-3-acetic acid. *Plant Physiol.* **133**: 794–802.
- Petrásek, J., and Friml, J.** (2009). Auxin transport routes in plant development. *Development* **136**: 2675–2688.
- Pollmann, S., Düchting, P., and Weiler, E.W.** (2009). Tryptophan-dependent indole-3-acetic acid biosynthesis by ‘IAA-synthase’ proceeds via indole-3-acetamide. *Phytochemistry* **70**: 523–531.
- Pollmann, S., Müller, A., and Weiler, E.W.** (2006). Many roads lead to “auxin”: Of nitrilases, synthases, and amidases. *Plant Biol (Stuttg)* **8**: 326–333.
- Pollmann, S., Neu, D., and Weiler, E.W.** (2003). Molecular cloning and characterization of an amidase from *Arabidopsis thaliana* capable of converting indole-3-acetamide into the plant growth hormone, indole-3-acetic acid. *Phytochemistry* **62**: 293–300.
- Quittenden, L.J., Davies, N.W., Smith, J.A., Molesworth, P.P., Tivendale, N.D., and Ross, J.J.** (2009). Auxin biosynthesis in pea: characterization of the tryptamine pathway. *Plant Physiol.* **151**: 1130–1138.
- Ritter, M.K., Padilla, C.M., and Schmidt, R.J.** (2002). The maize mutant *barren stalk1* is defective in axillary meristem development. *Am. J. Bot.* **89**: 203–210.
- Ronquist, F., and Huelsenbeck, J.P.** (2003). MrBayes 3: Bayesian phylogenetic inference under mixed models. *Bioinformatics* **19**: 1572–1574.
- Sakata, T., Oshino, T., Miura, S., Tomabechi, M., Tsunaga, Y., Higashitani, N., Miyazawa, Y., Takahashi, H., Watanabe, M., and Higashitani, A.** (2010). Auxins reverse plant male sterility caused by high temperatures. *Proc. Natl. Acad. Sci. USA* **107**: 8569–8574.
- Sanderson, M.J.** (2003). Molecular data from 27 proteins do not support a precambrian origin of land plants. *Am. J. Bot.* **90**: 954–956.
- Sekimoto, H., Seo, M., Dohmae, N., Takio, K., Kamiya, Y., and Koshiba, T.** (1997). Cloning and molecular characterization of plant aldehyde oxidase. *J. Biol. Chem.* **272**: 15280–15285.
- Sekimoto, H., Seo, M., Kawakami, N., Komano, T., Desloire, S., Liotenberg, S., Marion-Poll, A., Caboche, M., Kamiya, Y., and Koshiba, T.** (1998). Molecular cloning and characterization of aldehyde oxidases in *Arabidopsis thaliana*. *Plant Cell Physiol.* **39**: 433–442.
- Skirpan, A., Culler, A.H., Gallavotti, A., Jackson, D., Cohen, J.D., and McSteen, P.** (2009). BARREN INFLORESCENCE2 interaction with *ZmPIN1a* suggests a role in auxin transport during maize inflorescence development. *Plant Cell Physiol.* **50**: 652–657.
- Skirpan, A., Wu, X., and McSteen, P.** (2008). Genetic and physical interaction suggest that BARREN STALK 1 is a target of BARREN INFLORESCENCE2 in maize inflorescence development. *Plant J.* **55**: 787–797.
- Smith, L.G., and Hake, S.** (1993). A new mutation affecting tassel and ear morphology. *Maize Newsletter* **67**: 2–3.
- Stepanova, A.N., Robertson-Hoyt, J., Yun, J., Benavente, L.M., Xie, D.Y., Dolezal, K., Schlereth, A., Jürgens, G., and Alonso, J.M.** (2008). TAA1-mediated auxin biosynthesis is essential for hormone crosstalk and plant development. *Cell* **133**: 177–191.
- Strader, L.C., and Bartel, B.** (2008). A new path to auxin. *Nat. Chem. Biol.* **4**: 337–339.
- Sugawara, S., Hishiyama, S., Jikumaru, Y., Hanada, A., Nishimura, T., Koshiba, T., Zhao, Y., Kamiya, Y., and Kasahara, H.** (2009). Biochemical analyses of indole-3-acetaldoxime-dependent auxin biosynthesis in *Arabidopsis*. *Proc. Natl. Acad. Sci. USA* **106**: 5430–5435.
- Swofford, D.L.** (2000). *PAUP*: Phylogenetic Analysis Using Parsimony*. (Sunderland, MA: Sinauer Associates).
- Tao, Y., et al.** (2008). Rapid synthesis of auxin via a new tryptophan-dependent pathway is required for shade avoidance in plants. *Cell* **133**: 164–176.
- Tivendale, N.D., Davies, N.W., Molesworth, P.P., Davidson, S.E., Smith, J.A., Lowe, E.K., Reid, J.B., and Ross, J.J.** (2010). Reassessing the role of N-hydroxytryptamine in auxin biosynthesis. *Plant Physiol.* **154**: 1957–1965.
- Weijers, D., Sauer, M., Meurette, O., Friml, J., Ljung, K., Sandberg, G., Hooymaas, P., and Offringa, R.** (2005). Maintenance of embryonic auxin distribution for apical-basal patterning by PIN-FORMED-dependent auxin transport in *Arabidopsis*. *Plant Cell* **17**: 2517–2526.
- Woodward, A.W., and Bartel, B.** (2005). Auxin: Regulation, action, and interaction. *Ann. Bot. (Lond.)* **95**: 707–735.
- Wu, X., and McSteen, P.** (2007). The role of auxin transport during inflorescence development in maize, *Zea mays* (Poaceae). *Am. J. Bot.* **11**: 1745–1755.
- Yamada, M., Greenham, K., Prigge, M.J., Jensen, P.J., and Estelle, M.** (2009). The TRANSPORT INHIBITOR RESPONSE2 gene is required for auxin synthesis and diverse aspects of plant development. *Plant Physiol.* **151**: 168–179.
- Zhang, J., Nodzynski, T., Pencik, A., Rolcik, J., and Friml, J.** (2010). PIN phosphorylation is sufficient to mediate PIN polarity and direct auxin transport. *Proc. Natl. Acad. Sci. USA* **107**: 918–922.
- Zhao, Y.D., Christensen, S.K., Fankhauser, C., Cashman, J.R., Cohen, J.D., Weigel, D., and Chory, J.** (2001). A role for flavin monooxygenase-like enzymes in auxin biosynthesis. *Science* **291**: 306–309.
- Zhao, Y.D., Hull, A.K., Gupta, N.R., Goss, K.A., Alonso, J., Ecker, J.R., Normanly, J., Chory, J., and Celenza, J.L.** (2002). Trp-dependent auxin biosynthesis in *Arabidopsis*: Involvement of cytochrome P450s CYP79B2 and CYP79B3. *Genes Dev.* **16**: 3100–3112.